Journal of the Chinese Chemical Society, **1999**, *46*, 495-507

The Synthesis and Application of the Mesoporous Molecular Sieves MCM-41 — A Review

Hong-Ping Lin[a] (林弘萍), Yah-Ru Cheng[b] (鄭雅如), Chung-Rong Lin[c] (林宗榮), Feng-Yin Li[b] (李豐穎), Chang-Lin Chen[b] (陳長林), She-Tin Wong[b] (王志龍), Soofin Cheng[b] (鄭淑芬), Shang-Bin Liu[a] (劉尚斌), Ben-Zu Wan[c] (萬本儒), Chung-Yuan Mou[b]* (牟中原), Chin-Yuan Tang[d] (湯致遠) and Ching-Yen Lin[d] (林錦燕)

[a]*Institute of Atomic and Molecular Science, Academia Sinica, Taipei, Taiwan, R.O.C.*

[b]*Department of Chemistry, National Taiwan University, Taipei, Taiwan, R.O.C.*

[c]*Department of Chemical Engineering, National Taiwan University, Taipei, Taiwan, R.O.C.*

[d]*Department of Zoology, National Taiwan University, Taipei, Taiwan, R.O.C.*

We report a "delayed neutralization" process for the preparation of highly-ordered aluminosilicate MCM-41 molecular sieves with high thermal and hydrothermal stability, and sharp pore size distribution. However, the structural order and pore size are dependent on the carbon chain length. In the mixture surfactant systems, the pore size of the MCM-41 materials could be fine-tuned. The pore size can be extended from 2.5 to 4.5 nm by adding a suitable amount of hydrocarbons. The tubular morphology of the MCM-41 material of 0.3 to 10 micrometers diameter, where the wall consists of coaxial cylindrical pores of nanometers MCM-41, can be obtained by careful control of the surfactant-water content and the rate of condensation of silica. An optimum condition for automatic synthesis of the hierarchical TWT structure has been accomplished. The addition of 1-alkanols as cosurfactant would not only improve the order of the MCM-41 hexagonal structure but also promote the formation of micrometer-sized hierarchical materials, for example: tubules-within-tubule and uniform-sized hollow spheres of diameter 5.0 ± 1.0 μm. However, the inside of the micron spheres has intricate structures possessing various topological genus ranks. The MCM-41 is a good supporter for Molybdenum oxide catalysts. The rate of deactivation in the catalytic reaction of ethylbenzene dehydrogenation to styrene increases in the order: $M_T < M_P < SiO_2$. The physically mixed samples have higher catalytic activity than impregnated ones.

INTRODUCTION

The mesoporosity of the materials based on silica is arising as a new and exciting research field of great scientific and technological importance.[1] The ability of designing, both the size and wall surface characters of the pore, is important toward imposing a framework for tailoring catalytic activities and opto-electronic properties of further embedded clusters.[2,3] The accessible porosity can be utilized as a host for conducting or magnetic phases. The composite microstructure is then determined by the pore structure of the host. The electronic and magnetic properties can be tailored by altering the size, shape and relative concentrations. One could investigate the quantum size effects of clusters in semiconductors, magnetism, and superconductivity.[4,5] It is a new and exciting field to be explored simultaneously by chemists, physicists, and engineers.

In recent years, there have been extensive developments in the field of mesoporous aluminosilicate materials where the pores are of nanometer size. In particular, the discovery of the new family of mesoporous materials M41S by researchers at Mobil Oil Corp.[6,7] has attracted great attention by scientists. The pores are created by using surfactant-aluminosilicates self-assembly with surfactant organization as the templates and followed by calcination of the organic part. These mesoporous molecular sieves with adjustable and uniform pore sizes in the range of 1.5 to 10.0 nm, cover a new range of potential applications. These materials were synthesized with the cationic type surfactant-quaternary alkyltrimethylammonium salts $C_nH_{2n+1}(CH_3)_3N^+X^-$ and various silica sources (sodium silicates, tetraethyl orthosilicate, or silica gel) under hydrothermal conditions. In the solution and gel phases, the system exhibits various complex organizations: cylindrical micelles, hexagonal, cubic and lamellar phases. And it leads to various final periodic structures of the mesoporous materials, including MCM-41, MCM-48 (cubic), MCM-50 (lamellar), SBA-1, SBA-2, and SBA-3.[8] When one uses an anionic surfactant, some meso-structures of transition element oxides, such as TiO_2, can also be obtained.[9] In addition, Japanese workers have invented

mesoporous aluminosilicate FSM-16 with a similar structure as MCM-41 by combining Kanemite polysilicate and surfactants.[10,11]

One member of this series, MCM-41, which possesses a hexagonal arrangement of uniformly sized channel mesopores, has been the focus of most recent applications for use as catalysts, supporters and advanced materials. This field is exciting not only in the newly available size range of the pores but also in that the self-assembly involves the physics of soft matter that is very rich by itself.[12]

For the purpose of developing catalysis applications, various metals or oxides have been incorporated into the MCM-41 materials. Isomorphic substitution of trivalent cations such as Al, B, or Ga into the framework can result in the acidic catalyst.[13,14] For oxidation catalysis, early transition metals such as Ti, Zr, Fe or V have also been incorporated. The heteropolyacid-supported MCM-41 catalyst can also be made.[15,16] Using MCM-41 as a support for other more specific catalysts is also a new direction.[17] For example, the large MCM-41 channel can be used to immobilize the metalloporphrin oxidation catalyst. Many of these modified MCM-41 materials show a remarkable increase in catalytic activity.[18]

In this paper, we review our recent investigations of the MCM-41 materials in three parts.

In part 1, we have been involved in the study of both the physical chemistry of surfactant self-organization and the synthesis of mesoporous MCM-41 materials by inventing a new "delayed neutralization method".[19] We explored the effects of the variation of the surfactant and experimental factors on the formation of the MCM-41 materials. Factors examined include the chain length, counterion of the surfactant and the addition of cosurfactant (such as butanol or hexanol), and the rate of acidification, which were found to exert influence on the pore size, the structural order and the stability of the MCM-41 material. Moreover, the thermally stable MCM-41 samples could also be obtained at ambient temperature by the process.[20]

In Part 2, we report that the micron-sized hierarchical structures (i.e. tubules-within-tubule; TWT and hollow pillared spheres; HPS) could be successfully synthesized through soft and bendable intermediates at high alkalinity by careful control of the rate of acidification and the synthetic components. The MCM-41 nano-channels form the wall of these micrometer-sized hierarchical structures.[21] Thus, the preparation of mesoporous aluminosilicate materials was elevated to an exciting new level by having at least two length scales, micro- and nano-meters.[22-30] The ability to control structures in both length scales will have crucial impacts on catalysts, biomineralization, and design of the nanomaterials. In some previous works that report hierarchical order, the micron-scale structure is generated separately, for example by microemulsion or bacteria,[22,30] as a template for growing the nanostructure. Our process is however through a "liquid crystal phase transformation" mechanism. This then opens up whole new approaches to the design of hierarchical orders in inorganic nanomaterials because many other complex orders can be achieved in complex liquid crystalline phases and modern theories of complex fluids have developed to the extent that it can help us to understand the associated phase changes.

For optimizing the synthesis of these hierarchical structures, we designed an automatic production system for preparing large-scaled amounts of the TWT hierarchical structure with high yield (>95%) and uniformity in morphology.[31]

In part 3, we explore the application of our hierarchical MCM-41 as catalyst support. We use ethylbenzene dehydrogenation as the probe reaction. The catalytic dehydrogenation of ethylbenzene is an industrially important process for the manufacture of styrene.[32,33] The reaction was carried out in vapor phase at high temperatures (550 - 600 °C) with moderate conversions (usually about 50%) on iron oxide stabilized with several promoters and in the presence of superheated steam. In this review, we shall describe the performance of MCM-41 supported metal oxide catalysts with different morphologies in this reaction. The representative results for ethylbenzene dehydrogenation over MCM-41 supported molybdenum oxide catalysts are presented.

EXPERIMENTAL SECTION

Materials

The silica source was sodium silicate (27% SiO_2, 14% NaOH) from Aldrich. The quaternary ammonium surfactant compounds $C_nH_{2n+1}(CH_3)_3NX$ or $C_nH_{2n+1}NC_5H_5X$, X = Cl, Br or NO_3, were obtained from Aldrich, Merck or Tokyo Chemical Industry without further purification. Hydrocarbons (toulene and 1,3,5-isopropyl benzene) are from Acrôs. The source of aluminum was sodium aluminate from Riede-de Haën. Sulfuric acid, hydrochloric acid, acetic acid and nitric acid were obtained from Merck or Janssen Chimica.

Synthetic Procedure

The Preparation of Silica or Aluminosilicate MCM-41 Materials

To prepare pure-silica MCM-41 materials, sodium

silicate was added to a clear aqueous solution of the surfactant with stirring and a gel mixture was formed. After stirring for about 10 min at synthetic temperature, a proper amount of 1.20 M sulfuric acid was added into the gel mixture and the pH value was adjusted to about 8.0-11. Two different acidification rates were used afterward. One is to add the entire acid to the gel mixture at once - "immediate acidification"; the other is to add the acid drop by drop over about 30 min with a pipette - "gradual acidification". The hierarchical-ordered structure can only be obtained by gradual control of the rate of acidification,[21] which will be studied in detail in part 2. The molar ratio of the resulting gel composition is 1 SiO_2:(1-0.1) surfactant: 0.39 Na_2O:0.29 H_2SO_4:(1.5-0.1) 1-alkanol:(50-400) H_2O. Then, the mixture was stirred for 20 min and loaded into an autoclave and statically heated at 100 °C for 48-144 h. The resulting solid products were recovered by filtration, washed with deionized water and dried in air at room temperature or 100 °C. To remove the organic species occluded in the pores of MCM-41, the as-synthesized samples were calcined in air at 560 °C for 6 hr.

The aluminosilicate MCM-41 was synthesized with the same process mentioned above except that a suitable amount of sodium aluminate was added into the solution of surfactant in the first step.

The Catalytic Reaction Condition

Reactions were carried out in a continuous flow microreactor system at atmospheric pressure. The reactant, ethylbenzene, was injected continuously (2.72 mL/h) into the N_2 carrier gas stream (effluent flow rate = 30 mL/min) and the reaction product (gas and liquid) was analyzed off-line by a Shimadzu GC-7A gas chromatograph. Liquid product was collected by a condenser (10 °C) positioned at the outlet of the reactor.

Characterization

X-ray powder diffraction (XRD) data were collected on a Scintag X1 diffractometer using Cu Kα radiation (λ = 0.154 nm). N_2 adsorption-desorption isotherms were obtained at 77 K on a Micrometric ASAP 2010 apparatus. The sample was outgassed at 300 °C for about 6 hr in 10^{-3} torr prior to adsorption. The pore size distribution curves were obtained from the analysis of the desorption portion of the isotherms using the BJH (Barrett-Joyner-Halenda) method. The transmission electron micrographs (TEM) were taken on a Hitachi H-7100 operated at 100 keV. Scanning electron microscopy (SEM) was performed on a Hitachi S-2400, S-800 with an accelerating voltage of 20 keV.

RESULTS AND DISCUSSION

Part 1. A "Delayed Neutralization" Process for the Synthesis of MCM-41

Carbon Chain Length

First, we explored the effect of the carbon chain length of the surfactant on the MCM-41 materials by using the immediate acidification process. The x-ray diffraction (XRD) patterns of the calcined pure silica MCM-41 products synthesized from alkyltrimethylammonium salts (C_nTMAX, X = B for Br or Cl for Cl, n = 8 to 18) with carbon chain number varied from 8 to 18 (A to F in Fig. 1). It was clearly shown that the d_{100} value increases and the peaks become sharper as the carbon chain length increases. Furthermore, for MCM-41 materials prepared with $C_{16}TMAB$ and $C_{18}TMACl$ surfactants, there appear five XRD peaks indicating that the MCM-41 solids prepared by this new method are more ordered than those prepared by the previously reported methods.[34-39] The delayed neutralization process leaves more time for the micelles and silica polyanionic species to assemble into a more ordered structure. Neverthe-

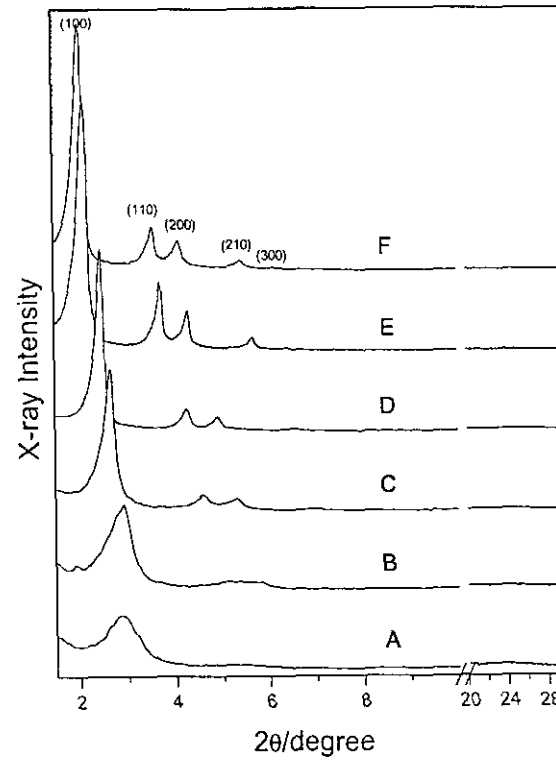

Fig. 1. X-ray powder diffraction patterns of calcined products prepared using the surfactants of different carbon chain length. A. C_8TMAB, B. $C_{10}TMAB$, C. $C_{12}TMAB$, D. $C_{14}TMAB$, E. $C_{16}TMAB$, F. $C_{18}TMACl$.

less, the structural order of the MCM-41 products decreases when the surfactants of shorter carbon chain length were used. This is accounted for by the weakening of interactions between the silica polyanionic species and the surfactants with shorter carbon chain length. Besides, the XRD baselines of all samples are flat at 2θ from 20 to 30°, implying that few microparticles of amorphous silica are formed using this method. The "delayed neutralization" process offers a convenient procedure to produce highly-ordered MCM-41 mesoporous materials with less amorphous silica impurity.

From the data of the N_2 adsorption-desorption isotherms of the calcined samples prepared with different surfactants, it reveals that there is a sharp increase in adsorbed volume at a certain relative pressure p/p_0, which corresponds to the capillary condensation in the mesopore of the materials. The pore size distributions calculated from N_2 desorption curves are quite narrow. The t-plots of these MCM-41 materials have close to zero intercepts, which indicate that the products have no microporous structures.[40,41]

Counterions

Table 1 compares the pore size, d-spacing and the wall thickness of the solids prepared with different carbon chain lengths, counterions and head groups of the surfactants. The pore-to-pore distance (a_0) was calculated from X-ray diffraction data. The wall thickness was determined by the difference between the distance (a_0) and pore size. These MCM-41 materials have a BET surface area in excess of 1000 m^2/g. The products prepared from surfactants with the same carbon chain length but different counterion and head group have almost the same pore size and d-spacing, which increase with the carbon chain length of the surfactant. This indicates that the counterions bound to the interface of the micelle of the surfactant are replaced by the silica polyanionic species during the synthetic process. The head group is relatively small, and the pore size is mainly dependent on the carbon chain length of the surfactant. The wall thickness of all the MCM-41 materials synthesized by this method is in the narrow range of 1.6 to 1.9 nm, which is quite independent of the surfactants. They shrink less (about 0.12 to 0.22 nm) after calcination and have a sharper pore size distribution (about 0.14 ~ 0.23 nm) than those previously reported. Transmission electron micrographs (TEM) of these calcined samples also illustrate the regular hexagonal array of mesoporous channels.[19]

Thermal and Hydrothermal Stability of the MCM-41 Materials

For testing the thermal and hydrothermal stability of the MCM-41 materials prepared from the "delayed neutralization" process, the samples after calcination were respectively re-calcined at 900 °C under air flow for 12 hr and in 100 °C hydrothermal condition for 24 hr. Although both of the samples after thermal and hydrothermal procedure show a d-spacing shrinkage (about 0.4 - 0.6 nm), these two samples still preserve the hexagonal MCM-41 structure (Fig. 2). It is clear that the mesoporous materials obtained from the new process could possess a higher stability than others reported in the literature. It is suggested that the more uniform and thicker walls make the MCM-41 materials more

Table 1. Effect of Surfactant Chain Length, Counterion, Head Group on MCM-41 Pore Size, XRD d_{100} Value, Hexagonal Unit Cell Parameter a_0 and the Wall Thickness

Surfactant	XRD d_{100} d-spacing/nm	a_0* /nm	N_2 pore size /nm	wall thickness /nm
$C_nH_{2n+1}(CH_3)_3NX$[a]				
C_{18}TMAB	4.30	4.96	3.23	1.73
C_{18}TMACl	4.28	4.94	3.18	1.76
C_{16}TMAB	3.96	4.57	2.87	1.70
C_{16}TMACl	3.98	4.59	2.87	1.72
C_{16}TMAN	4.00	4.61	2.86	1.75
C_{14}TMAB	3.61	4.17	2.56	1.61
C_{12}TMAB	3.31	3.82	2.21	1.61
C_{10}TMAB	3.15	3.64	1.92	1.72
C_8TMAB	2.90	3.35	1.67	1.68
$C_nH_{2n+1}NC_5H_5X$[b]				
C_{16}PyB	3.95	4.56	2.72	1.84
C_{16}PyCl	4.01	4.63	2.72	1.91
C_{12}PyCl	3.32	3.83	2.23	1.65

* $a_0 = 2d_{100}/\sqrt{3}$ as distance of nearest pore centers.
[a] alkyltrimethylammonium halide. [b] alkylpyridinium halide.

rigid and thermally stable.

Adding Cosurfactant for Improving the Hexagonal Structure[19]

The surfactant with shorter carbon chain length has less affinity to combine with the silica polyanionic species, thus the products synthesized from C_8TMAB, C_{10}TMAB and C_{12}PyCl-silicate systems have less well-resolved XRD patterns and the MCM-41 material has not yet been synthesized from C_6TMAB. Based on the principle of micelle formation, adding a proper amount of cosurfactant, such as butanol (BuOH) or hexanol (HeOH), could elongate the length of micelle to favor the interaction between micelles and silica polyanionic species.[42,43] Fig. 3 shows that the two diffuse XRD peaks of C_{10}TMAB products can change into three or four sharp peaks by adding BuOH or HeOH in a suitable alcohol/surfactant range. But the addition of BuOH or HeOH has no obvious effect on the structure prepared from the surfactant with the shorter carbon chain length (C_6TMAB or C_8TMAB). It is believed that the chain length of C_6TMAB or C_8TMAB is too short to form an energetically favorable liquid crystal structure.[44] We conclude that adding short chain alcohols (BuOH or HeOH) as cosurfactants can improve the formation of highly ordered hexagonal structure of MCM-41 for shorter carbon chain surfactants.

Fine Tuning the Pore Size of the MCM-41 with Mixture Surfactant[45]

We also tried to synthesize the MCM-41 materials at various mixing ratios from a mixed C_mTABr-C_nTABr system. In C_{18}TMAB-C_{14}TMAB components, the significant feature is that the d_{100}-spacing decreases smoothly as the molar ratio of C_{14}TABr increases. Fig. 4 demonstrates the d_{100}-spacings of as-synthesized samples and calcined samples; they are almost linearly decreasing with the increase of C_{14}TABr mole fraction. The d_{100}-spacing of the as-synthesized sample can be linearly adjusted from 4.70 nm to 3.85 nm by modifying the C_{18}TABr/C_{14}TABr mixing ratio. A similar linear trend is also observed in the trend of the pore size determined by nitrogen adsorption-desorption experiment, where the pore size ranges from 3.2 nm to 2.4 nm (bottom, Fig. 4). The pore size distributions in C_{18}TABr-C_{14}TABr mixed systems are fairly narrow and their full-width-half-maximum is less than 0.2 nm. The wall thickness is about 1.9 nm for all these samples. This indicates that the linearity of the d_{100}-spacing must be attributed to the mixed micelle template, not the silica. These linear relations in the C_{18}TABr-C_{14}TABr mixed system reflect ideal

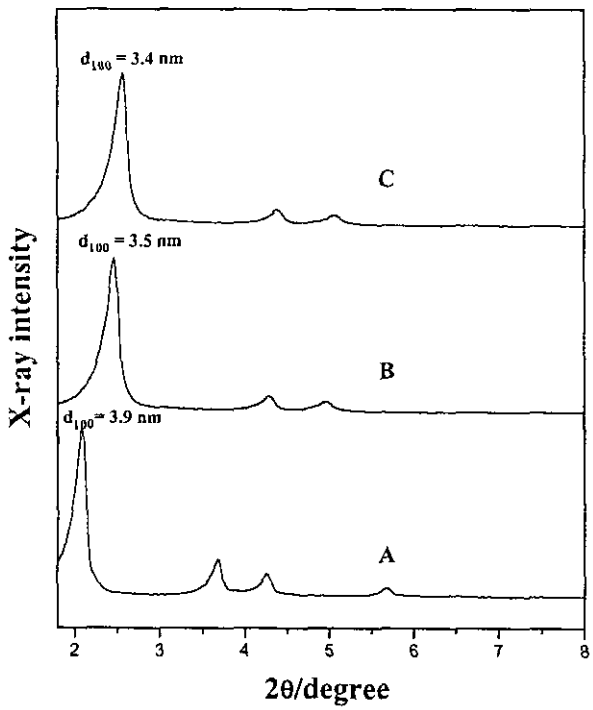

Fig. 2. X-ray diffraction patterns of the calcined products after different re-treatment conditions. A. calcined sample, B. after re-calcined at 900 °C, C. after re-hydrothermal reaction at 100 °C.

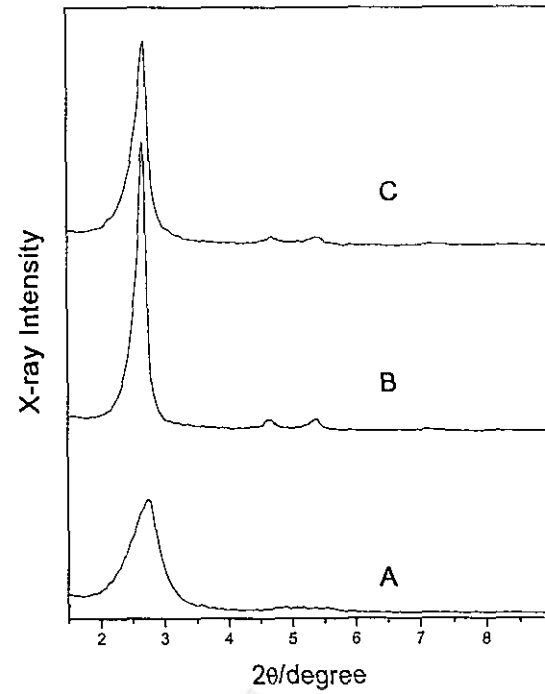

Fig. 3. X-ray powder diffraction patterns of the as-synthesized products prepared from different alcohol/C_{10}TMAB ratios using immediate acidification. A. BuOH/C_{10}TMAB = 0, B. BuOH/C_{10}TMAB = 0.65, C. HeOH/C_{10}TMAB = 0.25.

mixing, that is, the mixing ratio in the solution is the same as the mixing ratio in the mixed micelles. Such linearity allows a simple way to fine tune the pore size of MCM-41 materials.

The Addition of Hydrocarbons for Forming the Larger Pore Size MCM-41

In order to extend the application range of the mesoporous materials, expanding the pore size of the MCM-41 is an important determinant. Although using the longer carbon chain length of the surfactant could produce a larger pore size, the maximum value of the mesopore is only about 3.0 nm. In order to extend the large pore size, hydrocarbons were added into the reaction component. According to the data of the XRD and BJH pore size (Fig. 5), it is clear that the pore size of the mesoporous materials apparently increases with the triisopropylbenzene/C_{16}TMAB ratio at a ratio of less than 0.5. This is attributed to the solubilized triisopropylbenzene in the surfactant micelles for swelling the hydrophobic volume and pore size. When the ratio increases to about 0.5, the pore size no longer increases. It might be supposed that the micelle of the surfactant possesses a maximum absorption capacity. Adding other hydrocarbons (for example, toulene, trimethylbenzene, etc.) also can expand the pore size of the mesoporous materials. And this can offer another method for preparing the desired pore size of the mesoporous materials.

Synthesis of MCM-41 at Ambient Temperature

Our delayed neutralization method can also be employed at ambient temperature. Fig. 6 shows the x-ray dif-

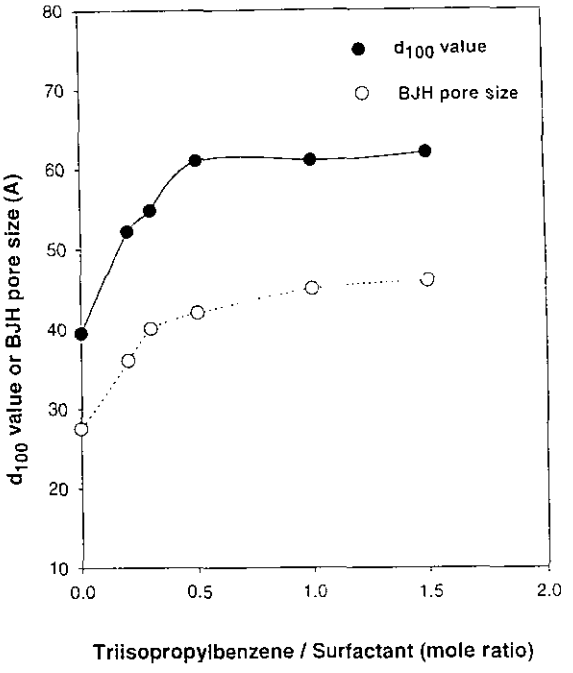

Fig. 5. The d_{100} value and BJH pore size of the MCM-41 materials prepared at various triisopropylbenzene/surfactant.

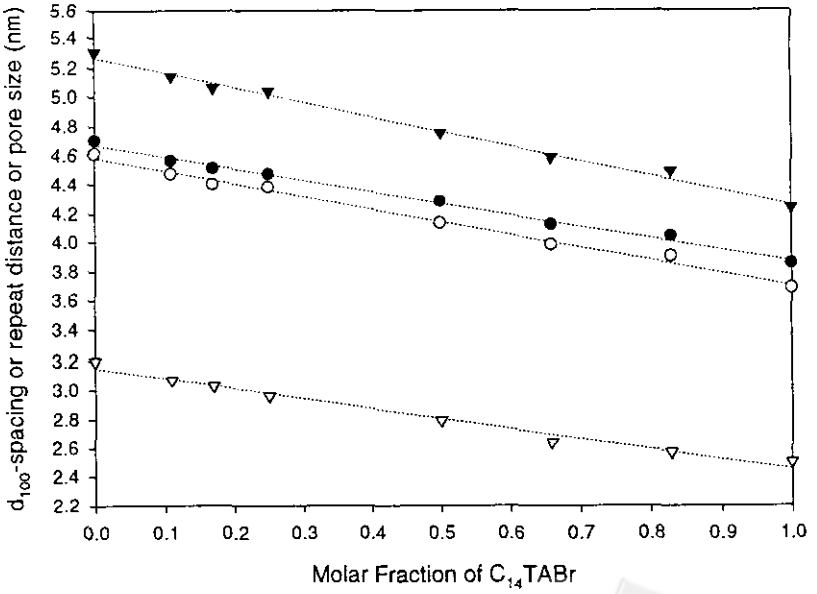

Fig. 4. The repeat distance, d_{100}-spacing and pore size of MCM-41 materials prepared from C_{18}TABr-C_{14}TABr-silicate system with different C_{18}TABr/C_{14}TABr ratio. (▼: repeat distance of calcined material, ●: d_{100}-spacing of as-synthesized material, O: d_{100}-spacing of calcined material, ∇: pore size of calcined material). These points are connected by the linear regression line. The molar ratio of the gel is 1 (C_{18}TABr + C_{14}TABr):1.8 SiO_2:0.55 Na_2O:0.45 H_2SO_4:140 H_2O.

fraction (XRD) patterns of calcined products synthesized at ambient temperature with aging time that varied from 0 to 30 days. As the aging time increases, the XRD peaks of the calcined material become sharper and more distinct. Four characteristic peaks of MCM-41 were detected in the samples with aging time equal or longer than 10 days. These results reveal that the condensation of silica walls was almost complete and stable MCM-41 structure was formed at ambient temperature after 10 days of aging. It was also found that the characteristic XRD patterns of the samples prepared with different aging times remain unchanged under prolonged heating at 900 °C in air for an additional six hours. Compared with the d_{100} of the samples calcined at 550 °C, there is only about 0.3 nm shrinkage. These results indicate that these samples synthesized at ambient temperature have high thermal stability. But we note that room temperature synthesis generally results in smaller d-spacing (about 0.5 to 0.6 nm differences) and smaller pore diameter of the products as compared to those with hydrothermal synthesis (Table 1). All samples synthesized by this method have BET surface areas of around 1100 m^2/g.

This new synthesis procedure is also suitable for the formation of aluminosilicate MCM-41. The ^{27}Al MAS NMR spectra of the products with different Si/Al (10-60) ratios show that there is only one peak at about 54 ppm in all as-synthesized samples, indicating that the aluminum atoms are incorporated in the tetrahedral sites in the framework of MCM-41.

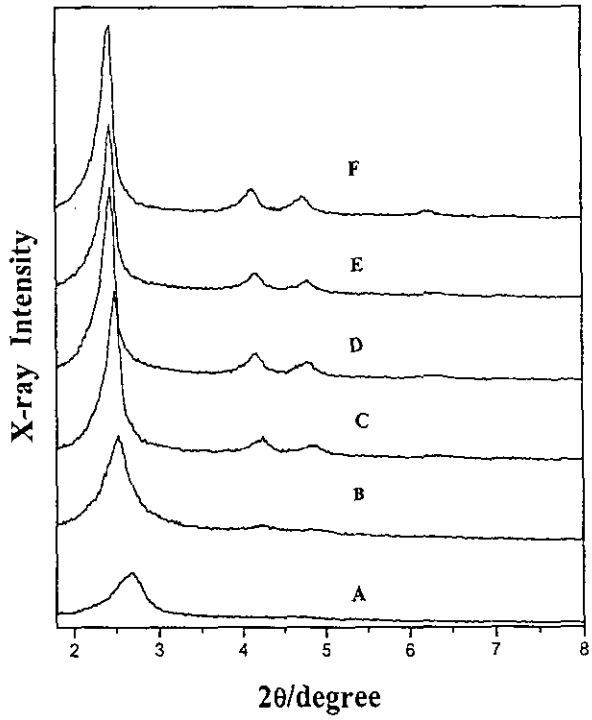

Fig. 6. X-ray powder diffraction patterns of the calcined products of the C_{16}TMAB-silicate system prepared at ambient temperature for different aging time. A. 0 day, B. 1 day, C. 5 days, D. 10 days, E. 20 days, F, 30 days.

Part 2. The Formation of Hierarchical Order in MCM-41

The Formation of a Tubules-within-tubule Hierarchical Structure

A tubule-shaped MCM-41 material of 0.3 to 3 micrometers diameter could be synthesized by careful control of the surfactant-water content and the rate of condensation of silica (gradually acidification) at high alkalinity condition. Fig. 7A showed a SEM micrograph of the high-yield and uniform tubules of MCM-41 synthesized with C_{16}TMAB. Transmission electron microscopy (TEM) of the sample (Fig. 7B) revealed that clear equidistant parallel lines arrange in a regular way along the tubular axis, with an

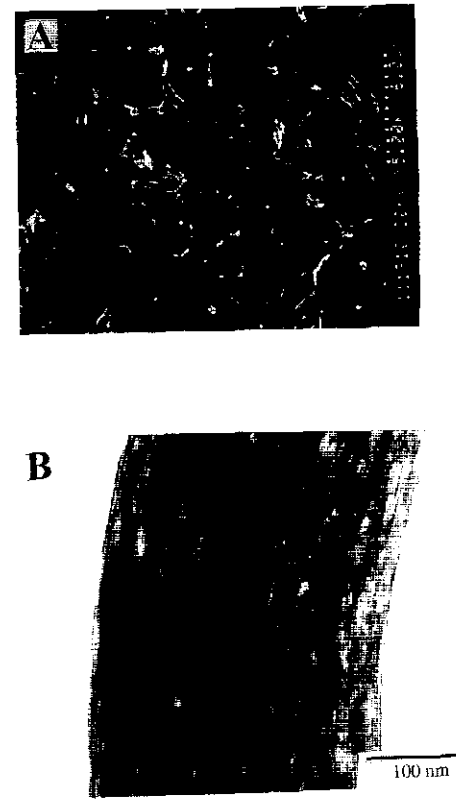

Fig. 7. The MCM-41 material obtained from the gel mixture with mole ratio, 1 Al_2O_3:75 SiO_2:30 Na_2O:35 C_{16}TMAB:6500 H_2O. A. Scanning electron microscopy (SEM) of the micro-sized tubular product B. Transmission electron micrograph of the tubular aluminosilicate MCM-41 material.

apparent average spacing at ~3.70 nm which is in reasonable agreement with the XRD result. Therefore, it was supposed that the wall of the tubule consists of coaxial cylindrical nanometer-sized channels characteristic of MCM-41 and the tubule is hollow. Examining many of the SEM micrographs, we find the tubular form represents >95% of the solid material.

The calcined product was further characterized by N_2 adsorption-desorption isotherm. It gives a BET surface area of about 1000 m^2/g. The pore size distribution shows an average pore size of about 2.6 nm and half-height width of 0.2 nm. The ^{27}Al nuclear magnetic resonance spectroscopy of the as-synthesized material shows a peak only at 54 ppm, indicating that all of the aluminum resides in the skeleton and in the tetrahedral environment.

To investigate the process of morphological change of this MCM-41 material, we examined the products at different stages of the acidification by x-ray diffraction (XRD) and scanning electron microscopy (SEM). The XRD pattern of the as-synthesized material at this early stage of neutralization is a poorly ordered hexagonal structure. The SEM micrograph of the sample shows, however, a layered lamellar-type structure. Gradual acidification to the mixture leads to an XRD pattern maintains the same hexagonal arrangement of MCM-41 with more distinct (110) and (200) peaks. The SEM micrograph reveals that the layers in sample A broke up into microtubules. After complete addition of acid, the sample completely transforms into tubules with a rather uniform diameter of ~ 0.3 μm and an average length ~ 5 μm.

The nearly complete transformation of the aluminosilicate at mild reaction condition into uniform size of hollow tubules leads us to propose a "liquid crystal phase transformation" mechanism for the formation of the new structure. In the beginning, with a high pH condition, the silicate/surfactant system was close to the lamellar/hexagonal phase boundary. A small extent of acidification results in a mixed lamellar/hexagonal phase in which layers of hexagonally arranged rod micelles are separated by bilayers of surfactants and water as shown in Fig. 8(A). It probably corresponds to the intermediate phase reported in the surfactant phase diagram. The layered structure could be stabilized by the electrostatic and entropic undulation repulsion force between the membrane layers.[46]

Since the membrane layers are intrinsically anisotropic, further acidification leading to condensation of silicates and charge imbalance on the membrane surface would favor curvature of the membrane only along one direction (Fig. 8(B)), the trans-rod direction. Further, neutralization would then bend the membrane completely into tubules as shown in Fig. 8(C). A "natural wavelength" of destabilization can thus be expected and leads to uniform diameters of tubules as we observed. The transformation of lamellar → ripple → tubular phase is in parallel with the known process in the formation of lipid tubules.[47-49] Recently, multilamellar lipid tubules have been observed through a first-order phase transition. In our case the driving force arises from the charge imbalance at surface associated with the condensation reaction of silicate-oxygen bond as pH value is lowered.

The higher order hierarchical silica structures observed in this work have been extensively documented in the ultrastructure of the siliceous skeletons of marine diatoms and radiolarians. The hollow tubular valve, with the large central area absent, of the diatom species *Annellus californicus*,[50] looks in fact strikingly similar to the hollow tubular structure we report here. Thus, we have demonstrated that such higher order biomimetic self-organization can be accomplished in laboratory chemistry.

Optimum Synthetic Conditions for Synthesizing the TWT MCM-41 Materials[31]

Although the synthesis procedures for tubular MCM-41 were presented in the previous report, many controlling factors were still not clear and need further optimization. A systematic study of the synthesis of tubular shape MCM-41 based on the composition of sodium silicate/aluminum hydroxide/C_{16}TMAB/water was carried out in an automatic batch type reactor. The effects of preparation conditions, e.g. mixing time, addition rate of H_2SO_4 (1.2 M) solution, stirring speed and reaction temperature, on the morphology of the MCM-41 products were investigated.

The quantitative comparisons of the effects of synthesis conditions on the tube formation and the crystallinity of

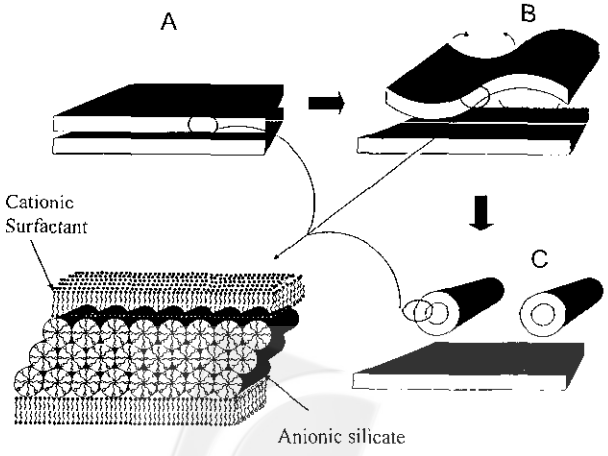

Fig. 8. Proposed mechanism for the formation of microtubular morphology of MCM-41.

Table 2. Characterization of Tubular Shape MCM-41 by XRD and SEM

Synthesis conditions						
Sample no.	Mixing time (min)	temp. (°C)	stirring speed (rpm)	H_2SO_4 add. rate (mL/h)	* fwhm of d(100) (2θ)	** Ratio of tubular shape (%)
A1	1	32	300	60	0.192	85
A2	10	32	300	60	0.188	95
A3	20	32	300	60	0.207	90
A4	30	32	300	60	0.189	10
B1	10	32	300	150	0.189	85
B2	10	32	300	120	0.188	90
B3	10	32	300	90	0.188	95
B4	10	32	300	60	0.204	95
B5	10	32	300	20	0.201	20
C1	10	38	300	60	0.174	50
C2	10	35	300	60	0.177	80
C3	10	32	300	60	0.188	95
C4	10	29	300	60	0.204	90
C5	10	26	300	60	0.154	10
D1	10	32	400	60	0.192	90
D2	10	32	300	60	0.188	95
D3	10	32	250	60	0.174	90
D4	10	32	200	60	0.169	70
D5	10	32	100	60	0.165	50

* Peak width at half maximum from XRD measurement.
** SEM observation.

MCM-41 were made in Table 2. The percentages of tubes (about 0.1 to 0.6 μm in diameters) among the synthesized products were accounted for by SEM pictures. The full width at half maximum (FWHM) of XRD patterns corresponding to the hexagonal (100) plane was used as a quantity for MCM-41 crystallinity. It can be observed when the ratios of tubular shape MCM-41 were less than or equal to 50% (most were particle shapes), the FWHM from XRD patterns was generally lower than those with higher ratios of tubular shape. For example, when the stirring speed was increased from 100 rpm to 400 rpm (No. D1 to D5 in Table 2) while other synthesis conditions were maintained as constants, the tubular shape ratios were increased from 50% to more than 90%, and the FWHM of the XRD increases from 0.165 to more than 0.174. Notice that the smaller FWHM of the XRD means better and more ordered hexagonal packing; in other words, the larger FWHM of tubular shape means less ordered crystallinity in MCM-41. It can be concluded from this study that the formation of tubes from lamellar membranes during an acidification process places constraints on the orderly hexagonal packing in MCM-41; therefore, the crystallinity of MCM-41 with a tubular shape is generally less than those of MCM-41 with a particle shape.

The tubular shape MCM-41 can be made at optimum synthesis conditions with an appropriate mixing system as illustrated in the Experimental Section with a mixing time for sodium silicate gel of about 10 min, an H_2SO_4 (1.2 M) solution addition rate of 60 to 120 mL/min, a stirring speed of about 300 rpm, and a mixing and acidification temperature of about 32 °C.

Adding 1-Alkanols for Promoting the Formation of the TWT Hierarchical Structure[51]

In the previous part, it was shown that adding a proper amount of medium carbon chain length 1-alkanols ($C_mH_{2m+1}OH$, C_mOH; $m \geq 4$) to the short carbon chain length cationic surfactant, quaternary ammonium halides $C_nH_{2n+1}TMAX$-silicate (n = 10-14, C_nTMAX, X = Br or Cl) systems can have a marked improvement in the hexagonal order. However, it has been argued (*vide supra*) that, by adding a proper amount of the C_mOH cosurfactant with $m \geq 4$, the hydrophobicity of the surfactant can be increased and hence favors the formation of hexagonal-lamellar intermediates, which are responsible for the formation of TWT hierarchical structure.

Upon adding a proper amount of C_4OH to the respective $C_{14}TMAB$ or $C_{12}TAMB$-silicate-H_2O system, the SEM results show that the morphology of the products would transfer from broken tubules or particles to distinct TWT hierarchical structures (Fig. 9) at rather high product yield (ca. 80-95%). The nanometer-scale physical properties of these hierarchical structured materials, such as the XRD patterns, d-spacings, pore diameters and BET surface areas are nearly identical with those listed in Table 1 for the same systems.

The TWT hierarchical structure can also be synthesized from other C_nTMAX-C_mOH-silicate systems (n = 12-14; X = Br or Cl; $m \geq 3$) by adding a proper amount of C_mOH with suitable carbon chain length to the desirable surfactant-silicate systems. It is found that, for the C_nTMAX-C_mOH-silicate system, the amount of C_mOH cosurfactant required in producing MCM-41 with TWT morphology decreases with increasing the carbon chain length of the surfactant. The desirable amount of added $C_mH_{2m+1}OH$ for the formation of lamellar-hexagonal liquid crystal intermediate necessary to synthesize the Tubules-Within-Tubule (TWT) hierarchical structure whose morphology and size can be controlled by varying the water content and the $C_mH_{2m+1}OH$/surfactant ratio.

Formation of the Hierarchical Hollow Spheres of Mesoporous Materials[52]

For the synthesis of MCM-41, when the intermediate structure becomes softer before extensive polymerization of silicates, other higher order organizations may also be controlled and formed, except for the TWT hierarchical struc-

ture. Here we use more cosurfactant butanol in addition to the surfactant C_{14}TMAB-silicate-water systems to adjust the bending elasticity of the membrane and helping with vesicle formation. Fig. 10A is a SEM micrograph of the hollow spheres made after calcination. The yield is rather high (> 98%) and the size is uniform, with an average diameter of 5.0 ± 1.0 μm. In Fig. 10A, one can see that some of the spheres are broken and they are always hollow with a pillar in the center. The spheres are intact after calcination; some are broken only when pressed hard by a spatula during SEM sample preparation. The XRD pattern of the material is typical for the hexagonal MCM-41 with d_{100} = 3.7 nm.

Fig. 10B shows an enlarged picture of one of the Pillar-within-Sphere (PWS) structures. Notice that the shell of the sphere appears rather thin, like eggshell, and a large amount of silica appears located at the center pillar. While most of the inside structures are of PWS form, even higher genus structures occur. Fig. 10C is a picture for the Fork-within-Sphere (FWS) structure. Fig. 10D shows a Cross-within-Sphere (CWS) structure. The abundance of the three types in this mesoporous sample is roughly in the order of PWS >> FWS ≅ CWS.

Part 3. The Application of the TWT Mesoporous MCM-41 Materials as the Heterogeneous Catalysts

The catalytic performance of various molybdenum loaded catalysts is compared in Fig. 11. Similar results are observed for these catalysts after regeneration in air at 500 °C. In both fresh and regenerated catalysts, MCM supported samples show higher steady state activity than SiO_2 supported ones, and physically mixed samples are better than impregnated ones. Molybdenum catalysts with tubular MCM support are particularly active. The steady state activity decreases in the order: Mo + M_T > Mo + M_P > Mo/M_P > Mo/SiO_2. The rate of deactivation seems to depend on the nature of the support, and increases in the order: M_T < M_P < SiO_2. The nomenclature of the catalysts is shown in the figure captions.

Characterization of Mo + M_T shows that they still preserve the basic properties of the support, namely bimodal pore size distribution, high surface area and pore volume. In other words, M_T is stable under thermal treatment in the presence of transition metal cations to at least 500 °C. The presence of metal oxide in the mesopore system of the physically mixed catalysts can be concluded from the de-

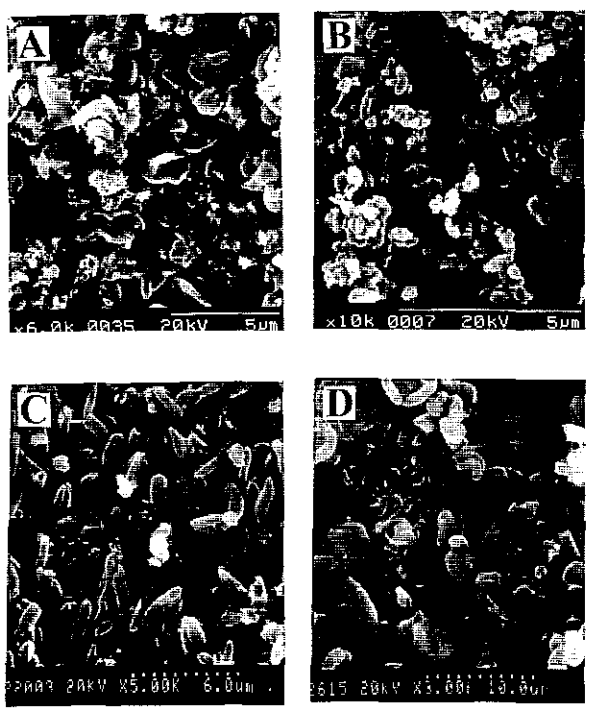

Fig. 9. The SEM micrographs of the calcined MCM-41 materials prepared from (C_{14}TMAB, C_{12}TMAB)-C_4OH-silicate systems. (A) C_4OH/C_{14}TMAB = 0; (B) C_4OH/C_{12}TMAB = 0; (C) C_4OH/C_{14}TMAB = 0.60 and (D) C_4OH/C_{12}TMAB = 0.85.

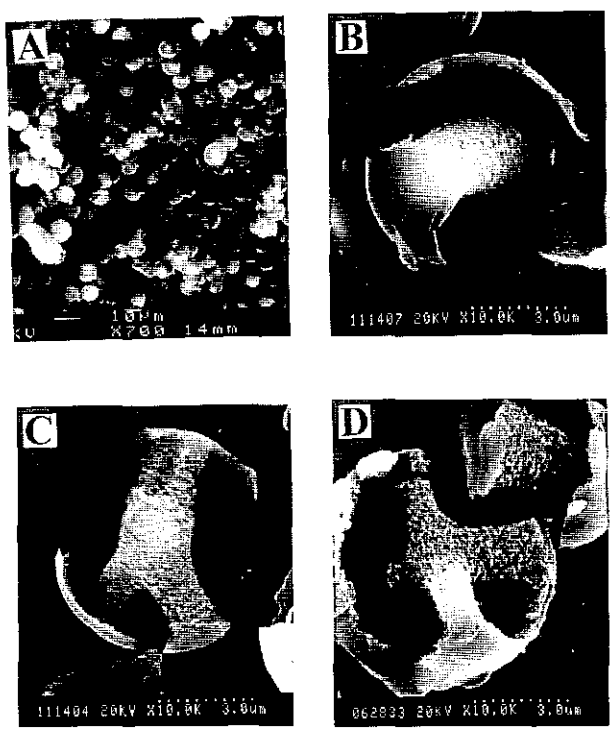

Fig. 10. The SEM micrographs of the calcined sample with different pillar shape, prepared from C_{14}TMAB-BuOH-silicate-H_2O gel composition. A. hollow spheres, B. pillar-within-sphere, C. fork-within-sphere, D. cross-within-sphere.

Table 3. Catalytic Performance of Mo-based MCM-41 Catalysts

Catalyst	Surface Area (m^2/g)	% Decay		10^{-3} × Activity (mol/h.g) Initial		Steady State	
		Fresh	Regen.	Fresh	Regen.	Fresh	Regen.
Mo + M_T	1005	20	18	6.34	5.37	3.07	2.99
Mo + M_P	959	29	31	5.88	5.08	2.60	2.20
Mo/M_P	779	31	22	4.34	4.04	1.53	1.48
Mo/SiO_2	377	48	47	5.26	4.74	1.12	0.93

The rate of catalyst deactivation is expressed in terms of the % decrease in initial conversion after 2 hr of reaction.
Initial and steady state activity was taken after 0.5 and 24 h of reaction on stream.

creased pore volume relative to the support. It is generally agreed that many oxides such as MoO_3 can be spontaneously dispersed onto the surface of supports to form a monolayer, because in these cases, the monolayer is a thermodynamically stable form.[53,54] In order to minimize the formation of multilayers, the Mo loading of the catalysts used is limited to 6% which is below the critical dispersion capacity of a monolayer of MoO_3 on the surface of even SiO_2. Consistently, XRD analysis does not reveal the existence of bulk MoO_3 on the surface of all the catalysts.

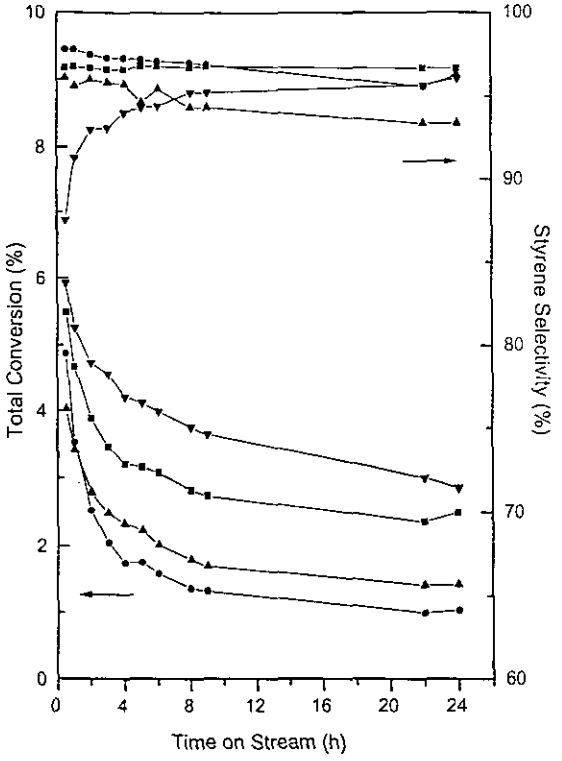

Fig. 11. Comparison of fresh Mo-loaded catalysts. Mo + M_P: Physically mixed catalyst with particulate MCM-41 as support; Mo/SiO_2: Impregnated catalyst with amorphous silica as support; Mo/M_P: Impregnated catalyst with particulate MCM-41 as support; Mo + M_T: Physically mixed catalyst with tubular MCM-41 as support.

Physical mixing is the simplest way to prepare a catalyst. The results of Mo + M_T catalyst in ethylbenzene dehydrogenation to styrene are summarized in Table 3, together with the data from other related systems for comparison purposes.

It is noted that Mo + M_T is the best performing catalyst with the highest steady state activity, which is a resultant of the initial activity and decay rate. The decay rate is the lowest even under the influence of intense acid-catalyzed side reactions known to produce coke, i.e oligomerization of styrene and cracking of ethylbenzene as revealed from its product distribution. Obviously, the high surface area and porosity of its framework have played a determining role in the catalytic reaction. The effect they exert can be looked at in three ways:

(i) Allows a better spreading of MoO_3 from external to its entire surface, and the concentration of reactive centers (possibly pairs of neighboring Mo sites) thus increases. This proposition is in-line with our TPR results as well.

(ii) Allows a better diffusion of reactant and product since each segment of the tubule's wall can be considered as a small particle of M_P. In this respect, the activity will be improved since the diffusion path (to the active site) is shorter than the case with particulate morphology.

(iii) Allows a better spreading of the reduced MoO_x species formed during the course of reaction through its entire surfaces, thus lowers the possibility of sintering in a reduced environment. The decay rate of Mo/SiO_2 catalyst is the highest since it is amorphous and has the lowest surface area.

CONCLUSIONS

The delayed neutralization process is a preferable

method for synthesizing highly-ordered silica and aluminosilicate MCM-41 with thick walls, high thermal and hydrothermal, and sharp pore size distributions. In this procedure, we could progressively improve the order and pore sizes in order to obtain desirable MCM-41 materials. Adding the 1-alkanol can improve the hexagonal structure order. Using the mixture surfactant systems provides a convenient method for fine-tuning the pore size. And the mesoporous materials with various pore dimensions, from 1.5 to 4.5 nm, could be readily synthesized by using the surfactants of different chain lengths or adding a suitable amount of hydrocarbons.

One can build the more complex hierarchical structures by careful control of the acidification rate to delay the formation of rigid structure. This may give us a new way to explore the many rich complex structures that are possible in a surfactant system and to form some new mesoporous structures. Adding alcohol as cosurfactant has resulted in many rich phase behaviors in ternary cosurfactant-surfactant-aqueous systems; it could open up a new way to synthesize other interesting hierarchical MCM-41 through various intermediate phases. This comprehensive study shows the capability in fine-tuning the structural ordering and morphology of mesoporous materials. Such capability would be useful in the future applications of MCM-41 materials in producing catalytic supports or embedded nanomaterials.

The ability to synthetically control the intricate hollow tubular and spherical forms of the aluminosilicate MCM-41 could find important applications in catalysis, separation technology and optoelectronics.[55] This process will be also suitable for manufacture of biomimetic hierarchical silica assemblies that may help one to understand the complex biomineralization process.

Mesoporous MCM-41 is well-known as a catalyst support for catalytic reactions involving bulk organic molecules due to its large surface area and pore size. However, by using a smaller reacting molecule like ethylbenzene which has no diffusion limitation in the pore systems (similar styrene selectivity in Mo/M_P and Mo/SiO_2 catalysts), we show for the first time in a mesoporous system the influence of structural morphology of a support on the performance of the catalyst. A similar phenomenon has been observed in the well-known microporous zeolite system. MCM-41 tubules possess both the pore structure and particle size advantages complementary to the many known zeolites.

ACKNOWLEDGMENT

This research was supported by the National Science Council of the R.O.C. (NSC 85-2113-31-M-002-032 cc) and the China Petroleum Corporation of the R.O.C.

Received January 18, 1999.

Key Words

M41S; MCM-41; Mesoporous molecular sieves; Delayed neutralization; Hierarchical order; Tubules; Hollow spheres.

REFERENCES

1. Schaefer. *MRS Bulletin* **1994**, *19*, 14.
2. Ozin, G. A.; Gil, C. *Chem. Rev.* **1989**, *89*, 1749.
3. Gillet, S. L. *Nanotechnology* **1996**, *7*, 168.
4. Stucky, G. D.; MacDaugall, J. E. *Science* **1990**, *247*, 669.
5. Awschalom, D. D.; DiVincenzo, D. P.; Smyth, J. F. *Science* **1992**, *258*, 414.
6. Kresge, C. T.; Leonowicz, M. E.; Roth, W. J.; Vartuli, J. C.; Beck, J. S. *Nature* **1992**, *359*, 710.
7. Beck, J. S.; Vartuli, J. C.; Roth, W. J.; Leonowicz, M. E.; Kresge, C. T.; Schmitt, K. D. C.; Chu, T-W.; Olson, D. H.; Sheppard, E. W.; Higgins, S. B.; Schlenker, J. L. *J. Am. Chem. Soc.* **1992**, *114*, 10834.
8. Stucky, G. D.; 11th International Zeolite Conference, Plenary Lecture, Seoul, Korea, **1996**.
9. Antonelli, D. M.; Ying, J. Y. *Angew. Chem. Int. Ed. Engl.* **1995**, *34*, 2014.
10. Yanagisawa, T.; Shimizu, T.; Kuroda, K.; Kato, C. *Bull. Chem. Soc. Japn.* **1990**, *63*, 988.
11. Inagaki, S.; Fukushima, Y.; Kuroda, K. *J. Chem. Soc. Chem. Comm.* **1993**, 680.
12. Gelbart, W. M.; Ben-Shaul, A. *J. Phys. Chem.* **1996**, *100*, 13169.
13. Luan, Z.; He, H.; Zhou, W.; Cheng, C.-F.; Klinowski, J. *J. Chem. Soc. Faraday Trans.* **1995**, *91*, 2955.
14. Cheng, C.-F.; Luan, Z.; Klinowski, J. *Langmuir* **1995**, *11*, 2815.
15. Tanev, P.; Chibwe, T. M.; Pinnavaia, T. J. *Nature* **1994**, *368*, 321.
16. Reddy, K.; Moudrakovski, M. I.; Sayari, A. *J. Chem. Soc. Chem. Comm.* **1994**, 1059.
17. Sayari, A. *Chem. Mater.* **1996**. *8*, 1840.
18. By now there is already a large patent literature providing a wealth of information about the use of MCM-41 as a catalysts for petrochemical applications. For a short review in published literature, see ref (17).

19. Lin, H. P.; Cheng, S.; Mou, C.-Y. *Microporous Mater.* **1996**, *10*, 111.
20. Lin, H. P.; Cheng, S.; Mou, C.-Y. *J. Chin. Chem. Soc.* **1996**, *43*, 375.
21. (a) Lin, H. P.; Mou, C.-Y. *Science* **1996**, *273*, 765. (b) Lin, H. P.; Cheng, S.; Mou, C.-Y. *Chem. Mater.* **1998**, *10*, 581.
22. Schacht, S.; Hou, Q.; Voigtmartin, I. G.; Stucky, G. D.; Schuth, F. *Science* **1996**, *273*, 768.
23. (a) Mann, S.; Ozin, G. A. *Nature* **1996**, *382*, 313. (b) Yang, H.; Coombs, N.; Sokolov, I.; Ozin, G. A. *Nature* **1996**, *381*, 589.
24. (a) Tanev, P. T.; Pinnavaia, T. J. *Science* **1996**, *271*, 1267. (b) Tanev, P. T.; Liang, Y.; Pinnavaia, T. J. *J. Am. Chem. Soc.* **1997**, *119*, 8616.
25. Grun, M.; Lauer, I.; Unger, K. K. *Adv. Mater.* **1997**, *9*, 254.
26. Hou, Q.; Feng, H.; Schuth, J. F.; Stucky, G. D. *Chem. Mater.* **1997**, *9*, 14.
27. (a) Yang, H.; Coombs, N.; Ozin, G. A. *Nature* **1997**, *386*, 692. (b) Ozin, G. A.; Yang, H.; Sokolov, I.; Coombs, N. *Adv. Mater.* **1997**, *9*, 662.
28. Mann, S.; Ozin, G. A. *Nature* **1996**, *382*, 313.
29. (a) Aksay, I. A.; Trau, M.; Mann, S.; Honma, I.; Yao, N.; Zhou, L.; Fenter, P.; Eisenberger, P. M.; Gruner, S. M. *Science* **1996**, *273*, 892. (b) K McGrath, M.; Dabbs, D. M.; Yao, N.; Aksay, I. A.; Gruner, S. M. *Science* **1997**, *277*, 552.
30. Davisd, S. A.; Burkett, S. L.; Mendelson, N. H.; Mann, S. *Nature* **1997**, *385*, 420.
31. Lin, C. R.; Wan, B. Z.; Lin, H. P.; Mou, C. Y. *Stud. Surf. Sci. Cat.* **1998**, accepted.
32. Lee, E. H. *Catal. Rev.* **1973**, *8*, 285.
33. Kaeding, W. W. *Catal. Rev.* **1973**, *8*, 307.
34. Monnier, A.; Schuth, F.; Huo, Q.; Kumar, D.; Margolese, D.; Maxwell, R. S.; Stucky, G. D.; Krishnamurty, M.; Petroff, P.; Firouzi, A.; Janicke, M.; Chmelka, B. F. *Science* **1993**, *261*, 1299.
35. Coustel, N.; Renzo, F. D.; Fajula, F. *J. Chem. Soc. Chem. Commun.* **1994**, 967.
36. Sayari, A.; Moudrakovski, I.; Danumah, C.; Ratcliffe, C. I.; Ripmeester, J. A.; Preston, K. F. *J. Phys. Chem.* **1995**, *99*, 16373.
37. Cheng, C. F.; Luan, Z.; Klinowski, J. *Langmuir* **1995**, *11*, 2815.
38. Beck, J. S.; Vartuli, J. C.; Kennedy, G. J.; Kresge, C. T.; Roth, W. J.; Schramm, S. E. *Chem. Mater.* **1994**, *6*, 1816.
39. (a) Chen, C. Y.; Li, H. X.; Davis, M. E. *Microporous Materials* **1993**, *2*, 17. (b) Chen, C. Y.; Xiao, S. Q.; Davis, M. E. *Microporous Materials* **1995**, *4*, 1.
40. Branton, P. J.; Hall, P. G.; Sing, K. S. W. *J. Chem. Soc., Chem. Commun.* **1993**, 1257.
41. Branton, P. J.; Hall, P. G.; Sing, K. S.; Reichert, W. H.; Schüth, F.; Unger, K. K. *J. Chem. Soc., Faraday Trans.* **1994**, *90*, 2965.
42. Candau, S.; Zaana, R. *J. Colloid Interface Sci.* **1981**, *84*, 206.
43. Almgren, M.; Swarup, S. *J. Colloid Interface Sci.* **1983**, *91*, 256.
44. Tiddy, G. J. *Phys. Rev.* **1980**, *57*, 1.
45. Cheng, Y. R.; Lin, H. P.; Mou, C. Y. Summited to *Langumuir*, **1998**.
46. Burckle, L. H. "Marine Diatoms" in "Introduction to Marine Micropaleontology" B. U. Haq, A. Boersna, Eds.: by Elsevier, **1979**, pp 245-275.
47. Schnur, J. M. *Science* **1993**, *262*, 1669.
48. Thomas, B. N.; Safinya, C. R.; Plano, R. J.; Clark, N. A. *Science* **1995**, *267*, 1635.
49. Radzihovsky, L.; Toner, J. *Phys. Rev. Lett.* **1995**, *75*, 4752.
50. Helfrich, W. Z. *Naturforsch* **1978**, *33a*, 305.
51. Lin, H. P.; Cheng, Y. R.; Liu, S. B.; Mou, C. Y. *J. Mater. Chem.* **1999**, in press.
52. Lin, H. P.; Cheng, Y. R.; Mou, C. Y. *Chem. Mater.* **1998**, *10*, 3772.
53. Xie, Y.-C.; Tang, Y-Q. *Adv. Catal.* **1990**, *37*, 1.
54. Gunther, S.; Marsi, M.; Kolmakov, A.; Kiskinova, M.; Noeske, M.; Taglauer, E.; Mestl, G.; Schubert, U. A.; Knozinger, H. *J. Phys. Chem. B* **1997**, *101*, 10004.
55. Zhao, D.; Yang, P.; Hou, Q.; Chmelka, B. F.; Stucky, G. D. *Current Opinion in Solid State and Mater. Sci.* **1998**, *3*, 111.